

# Particle RAIM

Shubh Gupta<sup>1</sup>, Grace Xingxin Gao<sup>2</sup>

<sup>1</sup>Department of Electrical Engineering, Stanford University

<sup>2</sup>Department of Aeronautics & Astronautics, Stanford University

**Abstract:** We propose a novel particle filter-based framework for robust state estimation and integrity monitoring in urban environments using GNSS and odometry measurements. Using a Gaussian mixture model (GMM) for computing particle weights, we develop an expectation-maximization algorithm for jointly inferring GMM weight parameters and a robust particle distribution of receiver state. From the inferred particle distribution and GMM, we determine the navigation system’s availability based on specified integrity requirements. Unlike traditional residual-based integrity monitoring algorithms that analyze measurement residuals from an estimated receiver position, we incorporate measurement residuals from multiple particles to estimate the receiver position and monitor integrity. Our method achieves small horizontal positioning errors compared to existing filter-based state estimation techniques on challenging simulated and real urban driving scenarios with multiple erroneous measurements. Through multiple simulations, we also show that our method determines system availability with comparable false alarms and missed-identifications to best-performing existing integrity monitoring approaches.

**Keywords:** Particle filter, Receiver Autonomous Integrity Monitoring, Global Navigation Satellite Systems, urban environment, mixture models, Sequential Monte Carlo, Expectation-Maximization.

## I. Introduction

Global Navigation Satellite System (GNSS) in urban environments is challenged by limited satellite visibility, signal attenuation, and multipath effects [1]. Such impairments to GNSS signals result in fewer measurements as compared to open-sky conditions as well as time-varying bias errors, or *faults*, in measurements. Therefore, safe navigation in urban environments requires addressing two challenges: accurately estimating the receiver position from the faulty measurements and determining the estimated position’s trustworthiness.

Integrity monitoring (IM) is employed by many navigation systems to both mitigate the effect of faulty measurements on receiver position estimation as well as determine the trustworthiness, or *integrity*, of the estimate [2]. Receiver Autonomous Integrity Monitoring (RAIM) algorithms identify and eliminate contaminated GNSS measurements using redundant information [3]. Using the remaining measurements, RAIM algorithms both provide a position estimate that is robust to measurement errors as well as inform the user when the provided position estimate is unreliable. However, most RAIM techniques have been developed for the aviation domain, and assume good satellite visibility and signal transmission. Therefore, state-of-the-art RAIM techniques cannot be directly used in urban environments, where multiple measurements may be contaminated by errors at any time instant and sufficient redundancy in measurements is unavailable.

### A. Prior Work

In this section, we discuss prior work on IM and robust state estimation. For the rest of the section, the state refers to both the receiver position and clock bias. First, we outline solution-separation and residual-based RAIM algorithms. Then, we discuss snapshot versus sequential IM techniques. Finally, we review existing particle filter-based sequential fault mitigation approaches and Bayesian algorithms for IM.

Existing RAIM algorithms are characterized as either solution-separation or residual-based approaches [4]. Solution-separation RAIM algorithms [5, 6, 7] mitigate measurement faults and provide integrity by considering multiple *fault hypotheses* that consider faults in different groups of measurements. For each fault hypothesis, solution-separation RAIM algorithms estimate the receiver state using a subset of all the available measurements. These algorithms then discard erroneous measurements by computing test statistics measuring the separation between the position solutions from the different fault hypotheses and the all-in-view solution. The final position solution is estimated using the remaining measurements. Additionally, the computed test statistics are analyzed to assess whether the estimated position solution is reliable. If the trustworthiness of the obtained position solution cannot be ensured, the navigation system is declared *unavailable*. However, specifying the different fault hypotheses is computationally intensive for more than two measurement faults, since the number of measurement subsets is combinatorial in the number of measurements and the number of faults considered [4].

On the other hand, residual-based RAIM algorithms [8, 9, 10] iteratively estimate the position and exclude measurement faults starting from the all-in-view position solution. These algorithms discard erroneous measurements by computing *residuals* for each measurement from the position estimate and a chi-squared distribution test statistic based on the residuals. Residual-based RAIM algorithms determine the navigation system availability by comparing the chi-squared test statistic associated with the final position estimate with a reference value based on specified requirements. However, residual-based RAIM is sensitive to the ratio of faulty and non-faulty measurements. For instance, if the ratio of faulty GNSS measurements is large, the estimated position could significantly deviate from the true position. Thus, discarding measurements based on the residuals computed from this position estimate can incorrectly exclude measurements, leading to significant positioning errors in the final position estimate.

Another categorization of IM algorithms is on the basis of the time instances considered. Many existing RAIM algorithms are *snapshot*, i.e., they estimate positions and determine integrity for each time instant independently [5, 11, 12]. Since snapshot algorithms do not incorporate measurement information from previous time instants, they require multiple measurements at each time instant to compute a robust position solution and determine the integrity of the system [3]. However, this is a restrictive requirement in urban environments where signals from multiple satellites may be blocked by buildings or trees [1].

Sequential integrity monitoring (SIM) algorithms combine filtering methods including, in some systems, measurements from inertial sensors with RAIM to capture temporal correlations in measurements. Grosch *et al.* [13] combined a Kalman filter with snapshot RAIM approaches for railway applications. Hewitson *et al.* [14] and Li *et al.* [15] combined an extended Kalman filter (EKF) with RAIM to detect step and ascending ramp fault profiles in GNSS measurements. Additionally, the authors derived protection levels using a mean position error bound for IM. Tanil *et al.* [16] utilized the innovation sequence of a Kalman filter for SIM. Kalman filter-based methods are useful for estimating the receiver position and monitoring integrity in scenarios containing few contaminated measurements. These methods approximate the probability distribution of the receiver state and the measurement error probability using a Gaussian distribution or a Gaussian distribution bound. However, this results in poor state estimation performance in urban environments since the probability of measurement errors in urban environments can be significantly non-Gaussian due to multipath and systematic receiver errors [1].

For modeling non-Gaussian state and measurement probability distributions, particle filters have been utilized in [17, 18] to track the receiver state using GPS measurements. A particle filter approximates the receiver state probability distribution using a finite set of samples (particles), and can model non-Gaussian probability distributions with multiple modes [19]. In [18, 20, 21], the authors construct multiple filters associated with different subsets of all the available measurements, and detect and remove faulty measurements using the logarithmic likelihood ratio test between the particles tracked by the constructed filters. However, constructing a large number of filters makes this approach computationally demanding and difficult to scale for multiple measurement faults. In recent work, [22] proposed grouping different fault hypotheses to reduce computation in solution-separation RAIM algorithms. However, scaling this approach becomes impractical in urban environments where multiple measurements might be contaminated with errors. Multiple prior works [23, 24, 25] have proposed techniques to identify and exclude multipath-degraded or non line-of-sight (NLOS) GNSS measurements using a particle filter and a 3D model of the environment. However, procuring and maintaining such a 3D model of the environment on a large scale is difficult, which limits the practical applications of these approaches.

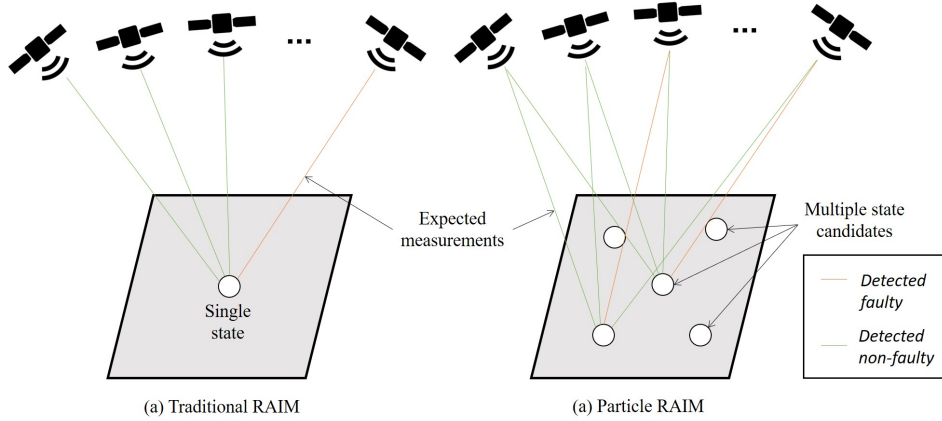


Figure 1: Positioning using traditional RAIM algorithms (left) versus proposed Particle RAIM algorithm (right). Traditional RAIM algorithms estimate the receiver state by identifying a non-faulty subset of measurements. Instead, Particle RAIM robustly captures the state probability distribution by simultaneously considering measurement subsets associated with multiple candidate states within a particle filter probability distribution.

Traditional RAIM	Particle RAIM
Estimates the receiver state and covariance	Estimates a multimodal probability distribution of the receiver state as particles
Mitigates measurement faults separately from estimating the state	Jointly mitigates measurement faults and computes the state probability distribution within a single Bayesian framework
Detects and excludes the faulty measurements	Tracks multiple measurement fault hypotheses (implicitly) through particles

Table 1: Differences between traditional RAIM and the proposed Particle RAIM algorithm.

In another line of work, Pesonen [26] proposes a fully Bayesian framework for RAIM in urban environments. The framework is described for a variety of Bayesian filters which track the receiver state along with multipath bias indicators for all the available GNSS measurements. The integrity monitor in Bayesian RAIM declares the navigation system ‘unavailable’ when the position error exceeds a specified alarm limit. To determine the system availability, Bayesian RAIM derives measures of accuracy and integrity risk using the filter probability distribution and compares them against specified integrity requirements. The approach is derived from Bayesian principles and is applicable to a wide variety of filtering algorithms.

## B. Our Approach

In this paper, we build upon our prior work on the Particle RAIM algorithm [27] that incorporates GNSS and odometry measurements for robust positioning and IM in urban environments. Like existing RAIM algorithms, Particle RAIM both mitigates measurement faults to estimate a robust position and determines the system availability for IM. However, instead of utilizing measurement residuals from the estimated position such as in residual-based RAIM, Particle RAIM mitigates faults through residuals computed across multiple particles in a particle filter probability distribution 1. For IM, we determine the system availability by building on the Bayesian RAIM framework [26]. Our IM algorithm specifically accounts for the probability of positions that are distant from the estimated position.

Particle RAIM jointly estimates the state and mitigates measurement faults within a Bayesian framework. In sce-

narios with multiple measurement faults, large positioning errors may result from estimating the receiver position based on an identified subset of non-faulty measurements, such as in [5, 8]. Therefore, our Bayesian framework considers a multimodal probability distribution of the state represented using particles which are likely under different groups of GNSS measurements. In scenarios with multiple equally likely receiver states, we assign similar probabilities to positions that are likely under different measurement subsets. We evaluate the probability of each position using a Gaussian mixture model (GMM) likelihood [28] over the GNSS measurements. The GMM likelihood is characterized by a weighted sum of multiple probability distribution components totaling the number of available measurements at the time instant. Each component in our GMM represents the conditional probability distribution of observing a single GNSS measurement from a position. For each GMM component, the associated weight coefficient is derived at runtime from the particle distribution. Our GMM likelihood assigns high probability to positions that are supported by measurements with high weight coefficients. Therefore, Particle RAIM mitigates measurement faults by assigning low values to the weight coefficients of GMM components corresponding to faulty GNSS measurements.

We next describe the key features of our algorithm. Similar to prior work in particle filter-based SIM, we leverage the correlation in measurements across time instants by (1) adopting a particle filter for state estimation and (2) using odometry measurements from an inertial measurement unit (IMU). To jointly infer the particle weights and GMM weight coefficients, we develop an iterative scheme based on expectation-maximization (EM) [29]. Inspired by residual-based RAIM [8], our algorithm mitigates faults using GNSS measurement residuals from the receiver state particle distribution. To estimate a robust state probability distribution, we derive a cost function based on the measurement residuals and iteratively update the particle weights and the GMM weight coefficients. We determine the system availability by computing measures of integrity risk and accuracy similar to [26]. However, our approach differs from [26] in that we compute integrity risk using the GMM likelihood instead of the particle distribution. We declare our system available if the computed integrity risk and accuracy meet prespecified requirements.

Particle RAIM provides several advantages over prior approaches that handle multiple measurement faults in urban environments. Table 1 provides a comparison with traditional RAIM algorithms. Unlike the existing particle filter-based SIM approaches that exhibit a combinatorial growth in computation with increasing number measurements and measurement faults, our approach scales linearly in computation with the number of measurements. This is due to our iterative approach for directly mitigating multiple faults instead of considering different subsets of measurements. Unlike Bayesian RAIM [26], our approach does not require a known transition model of measurement faults across different time instants. Furthermore, we derive the integrity risk through the GMM likelihood to account for the multi-modal and heavy-tailed nature of the position probability distribution, unlike the particle-based approach in [26].

The contributions of our work are five-fold:

1. We present a novel Bayesian state estimation framework that is robust to multiple GNSS measurement faults at each time instant. We develop a particle weighting scheme that integrates particle filter [19] with residual based RAIM to mitigate measurement faults.
2. We design a novel Gaussian mixture based likelihood model of the probability distribution of GNSS measurements from a receiver position. Each component in the likelihood model corresponds to a single measurement and is associated with a weight coefficient. We develop an iterative scheme based on the EM algorithm [29] to jointly infer the weight coefficients and particle weights that reduce the impact of faulty measurements on state estimation.
3. Through our iterative scheme for mitigating measurement faults, we create an efficient algorithm that scales linearly in computation with the number of measurements.
4. For determining availability, we derive an expression for integrity risk that leverages our GMM likelihood of GNSS measurements. Unlike existing IM approaches that use the particle filter distribution, our approach accounts for the tail-end probabilities of the estimated receiver position.
5. We have validated our approach on simulated and real-world driving scenarios with various noise profiles imitating urban environments. As compared to existing particle filter and Kalman filter based SIM tech-

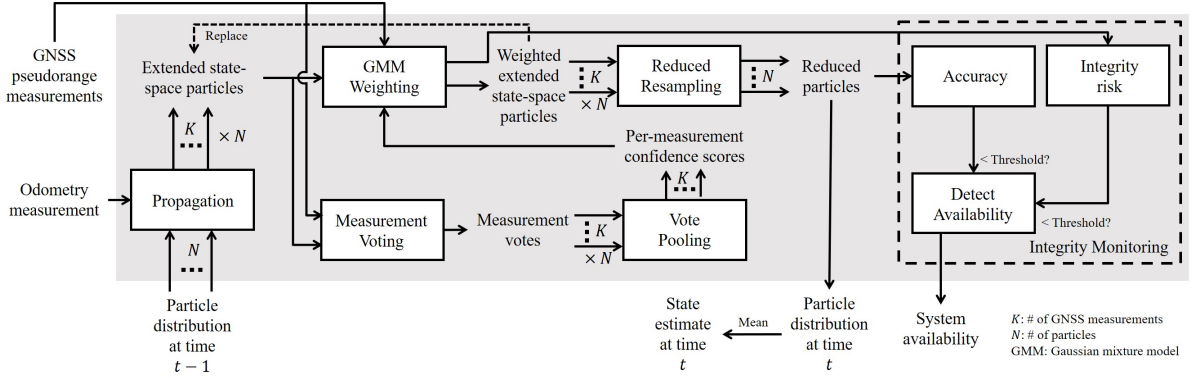


Figure 2: Architecture of Particle RAIM algorithm. The probability distribution of the vehicle state is estimated as a set of weighted particles in a particle filter. The Propagation step generates replicas of each particle for all GNSS measurements, denoted as extended state-space particles, and propagates them using an odometry-based motion model. For each extended state-space particle and its associated GNSS measurement, The Measurement Voting step computes the probability of observing the measurement residual under a chi-squared distribution, denoted as a measurement vote. Vote Pooling step combines the votes obtained across particles to compute weighting coefficients, or confidence scores, in a GMM measurement likelihood model where each confidence score is associated with a single measurement probability component in the GMM. Then, a GMM measurement likelihood is constructed using the confidence scores and weights associated with all extended state-space particles are updated. The process is then repeated for a fixed number of iterations using the new extended state-space particles. Finally, the particles are resampled and reduced to the original size to obtain the new particle distribution as well as the state estimate. For integrity monitoring using the state estimate, system availability is determined by computing measures for integrity risk as well as accuracy and comparing them against prespecified thresholds.

niques, our algorithm attains smaller positioning errors as well as few false alarms and missed identifications in determining system availability.

The rest of the paper is organized as follows: Section II discusses the proposed Particle RAIM algorithm in detail. Section III details validation experiments and comparisons with existing techniques on both simulated and real-world data. Section IV summarizes our work and provides concluding remarks.

## II. Particle RAIM Framework

This section details our proposed framework. First, we describe the problem setup for our state estimation algorithm. Then, we illustrate the individual components of our framework. Finally, we theoretically analyze the computation time requirement of our approach. Fig. 2 outlines the different components in Particle RAIM:

1. The Propagation step receives as input the previous time particle distribution of receiver state and the odometry measurement and generates as output propagated particles in the *extended state-space*. The extended state-space consists of both the receiver state and an integer denoting one GNSS measurement associated with the particle.
2. The Iterative Weighting step receives as input the extended state-space particles and the GNSS measurements and infers the particle weights and GMM weight coefficients in three steps: First, the Measurement Voting step computes probabilistic votes from the extended state-space particles to their associated GNSS measurements. Next, the Vote Pooling step combines the probabilistic votes to obtain the GMM weight coefficients, or confidence scores. Finally, the GMM Weighting step updates the particle weights using the new GMM constructed from the weight coefficients. The process is then repeated for a fixed number of iterations, or till convergence.
3. The Reduced Resampling step receives as input the extended state-space particles and their computed weights and generates a new set of particles in the receiver state space.

4. For IM, we compute the measures of Accuracy and Integrity Risk using the particles and the GMM likelihood. Then, we determine the System Availability by comparing the obtained accuracy and integrity risk against prespecified requirements.

While our approach focuses on GNSS and odometry measurements, it can be generalized to incorporate measurements from other sensors, such as camera or LiDAR, in computing the particle weights.

### A. Problem Setup

Consider a vehicle navigating in an urban environment using GNSS and odometry measurements. We denote the true state vector of the vehicle at time  $t$  as  $x_t$ , and the overall trajectory as  $\{x_t\}_{t=1}^T$ , where  $T$  denotes the total duration of the vehicle's trajectory. For generality, we do not restrict the state vector  $x_t$  to have a specific form and instead assume that it consists of various quantities such as the vehicle's position coordinates, heading angles, receiver clock errors, linear velocities, and yaw rates. The  $k$ th GNSS pseudorange measurement acquired at time  $t$  is denoted by the scalar value  $\rho_t^{(k)}$ . At time  $t$ , the vehicle acquires a set of  $K_t$  GNSS pseudorange measurements  $M_t = \{\rho_t^{(k)}\}_{k=1}^{K_t}$  and odometry measurement  $u_t$ . The probability distribution  $\pi_t$  of the vehicle state is approximated by a particle filter as

$$\pi_t = P(x_t|x_{t-1}, M_t, u_t) \approx \hat{\pi}_t = \sum_{i=1}^N w_t^{(i)} \delta(x = x_t^{(i)}), \quad (1)$$

where

$\hat{\pi}_t$  denotes the approximate state probability distribution represented using particles;

$x_t^{(i)}$  denotes the state of the  $i$ th particle;

$w_t^{(i)}$  denotes the weight of the  $i$ th particle such that  $\sum_{i=1}^N w_t^{(i)} = 1$ ;

$\delta(x = x_t)$  denotes the Dirac delta function [30] that assumes the value of zero everywhere except  $x_t$ ;

$N$  is the total number of particles.

The expression for  $\pi_t$  assumes the Markov property among state variables  $(x_1, \dots, x_t)$ , which means that  $x_t$  depends on the past states and measurements  $(x_1, \dots, x_{t-1}, M_1, \dots, M_{t-1}, u_1, \dots, u_{t-1})$  only through  $x_{t-1}$ . Hence, the conditional probabilities  $P(x_t|x_{t-1}, M_t, u_t)$  and  $P(x_t|x_1, \dots, x_{t-1}, M_1, \dots, M_t, u_t)$  are equivalent. The particle weights  $\{w_t^{(i)}\}_{i=1}^N$  are initialized uniformly to be  $N^{-1}$ . Following the methodology in standard filtering algorithms [31] and applying Bayes theorem with independence assumptions on  $M_t, u_t$ , the probability distribution can be factorized as

$$\begin{aligned} P(x_t|x_{t-1}, M_t, u_t) &\propto P(M_t|x_t, x_{t-1}, u_t) \cdot P(x_t|x_{t-1}, u_t) \\ &\propto \underbrace{P(M_t|x_t)}_{L_t(x_t)} \cdot \underbrace{P(x_t|x_{t-1}, u_t)}_{\hat{\pi}_t}, \end{aligned} \quad (2)$$

where

$L_t(x_t)$  can be interpreted as the likelihood of receiving the set of measurements  $M_t$  at time  $t$  from state  $x_t$ ;

$\hat{\pi}_t$  is the propagation term which denotes the predicted probability distribution at time  $t$  that is approximated using the particle probability distribution at previous time  $\hat{\pi}_{t-1}$  and odometry measurement  $u_t$ .

In Particle RAIM, we consider the joint tasks of state estimation and fault mitigation using an extended state-space  $(x, \chi)$  of particles, where  $\chi = k \in \{1, \dots, K_t\}$  denotes an integer corresponding to the  $k$ th GNSS measurement in the measurement set  $M_t$ . The value of  $\chi$  is assigned to each extended state-space particle at the time of its creation in the propagation step, and remains fixed until the state-space of the particles is reduced to just the vehicle state-space in the reduced resampling step. The extended state-space particles are used in the iterative weighting step to determine the weight coefficients in the GMM likelihood as well as to compute the particle weights.

We next provide details about each algorithmic step in Particle RAIM.

## B. Propagation Step

The propagation term is approximated by applying a Markov chain transition using known system dynamics and odometry measurement  $u_t$  on the extended state-space particle distribution computed from the particle distribution  $\hat{\pi}_{t-1}$  at the previous timestep  $t-1$ . For computing the extended state-space particles from  $\hat{\pi}_{t-1}$ , we first generate uniformly weighted  $K_t$  copies of each particle  $x_{t-1}^{(i)}$ , each corresponding to a different value of  $\chi = \{1, \dots, K_t\}$ . We then propagate the extended state-space particles  $(x)_{t-1}^{(i,\chi)}$  via the state dynamics to get the propagation term

$$x_t^{(i,\chi)} = f(x_{t-1}^{(i,\chi)}, u_t) + \epsilon_f^{(i,\chi)} \quad \forall \chi = \{1, \dots, K_t\}, \quad (3)$$

$$\tilde{\pi}_t^{(i)} = \sum_{k=1}^{K_t} K_t^{-1} \delta(x = \tilde{x}_t^{(i,\chi=k)}), \quad (4)$$

$$\tilde{\pi}_t \approx \sum_{i=1}^N w_{t-1}^{(i)} \tilde{\pi}_t^{(i)}, \quad (5)$$

where

$f : \mathcal{X} \times \mathcal{U} \rightarrow \mathcal{X}$  is the function to propagate state  $x \in \mathcal{X}$  using odometry  $u \in \mathcal{U}$  based on system dynamics;

$\epsilon_f^{(i,\chi)} \sim \mathcal{N}(0, \sigma_f^2)$  denotes the stochastic term in propagation of each extended state-space particle;

$x_t^{(i,\chi=k)}$  denotes an extended state-space particle associated with measurement  $k$ , and is constructed by propagating the  $i$ th particle;

$\tilde{\pi}_t^{(i)}$  denotes the particle distribution consisting of  $K_t$  propagated equally-weighted replicas of  $i$ th particle.

Next, we compute the measurement likelihood model and update the weights associated with each particle in the weighting step.

## C. Iterative Weighting Step

In standard filtering schemes, the measurement likelihood model is designed with the assumption that all the measurements are independent of each other and follow the likelihood model [31]

$$L_t(x_t) = \prod_{k=0}^{K_t} P(\rho_t^{(k)} | x_t) \quad (6)$$

Existing filtering algorithms for GNSS-based navigation [32, 26, 33] model the probability  $P(\rho_t^{(k)} | x_t)$  associated with the  $k$ th measurement at time  $t$  for  $x_t$  as a Gaussian distribution. The mean parameter of the distribution  $\hat{\rho}_{x_t}^k$  is set as the expected value of the  $k$ th pseudorange measurement from  $x_t$  assuming known satellite position, and standard deviation  $\sigma_{x_t}^k$  is based on Dilution of Precision (DOP) [34] or is empirically computed. The overall measurement likelihood hence becomes

$$L_t(x_t) = \prod_{k=0}^{K_t} \mathcal{N}(\rho_t^{(k)} | \hat{\rho}_{x_t}^k, (\sigma_{x_t}^k)^2), \quad (7)$$

However, this likelihood model inherently assumes a unimodal probability distribution of  $x_t$ , and therefore, has a tendency to over simplify the measurement errors when faults occur in multiple GNSS measurements. For example, a large bias in one measurement, which is common in a multipath degraded environment, may severely reduce the likelihood of a particle even if other measurements support it. Therefore, the likelihood needs to be modeled so that fault in one measurement does not have a dominating effect on the overall measurement likelihood. Additionally, different subsets of measurements can support different regions in the position space and must be modeled as such.

Hence, we model the likelihood instead as a Gaussian mixture model (GMM) which has additive contributions of each measurement towards the likelihood unlike the multiplication of individual likelihoods in the former model. Each measurement component in the GMM likelihood is associated with a weight, or *confidence score*, which controls the amount of impact that component has on the overall likelihood. Given a few faulty measurements, an assignment of low confidence scores to their components in the GMM would lower the impact that faulty measurements have on the computed particle weights. The mixture model based likelihood is expressed as

$$L_t(x_t) = \sum_{k=1}^{K_t} \gamma_k \mathcal{N} \left( \rho_t^{(k)} | \hat{\rho}_{x_t}^k, (\sigma_{x_t}^k)^2 \right) \quad \text{s.t.} \quad \sum_{k=1}^{K_t} \gamma_k = 1, \quad (8)$$

where  $\gamma_k$  is the confidence score associated with  $k$ th measurement that scales the individual probability distribution components to enforce a unit integral for the probability distribution. The measurement component for the  $k$ th measurement in the GMM assigns similar probabilities to all the positions  $x_t$  which generate expected pseudorange measurement values  $\hat{\rho}_{x_t}^k$  that are similar to each other. In the particle distribution, a large weight can be assigned to a particle through the GMM likelihood in multiple scenarios. For instance, a high value of particle weight can be computed when a few measurement components with high confidence scores support the particle, or alternatively the particle is supported by multiple measurement components with low confidence scores. Therefore, the GMM induces a multi-modal probability distribution over the state, with peaks at positions supported by different subsets of component measurements. Note that the probability distribution of the state  $x_t$  using GMM is multimodal for any configuration of the confidence scores, if the individual measurement components disagree with each other. The values of confidence scores, however, decides the relative confidence between the modes, i.e., for the same values of standard deviation, the mode of the component with higher confidence score has a higher probability value associated with it [28].

Using the proposed GMM likelihood, we jointly determine the values for the measurement confidence scores  $\{\gamma_k\}_{k=1}^{K_t}$  and particle weights  $\{w_t^{(i)}\}_{i=1}^N$  using a three-step iterative approach. Our approach is based on the EM algorithm for GMM [35] and consists of the measurement voting, vote pooling and GMM weighting steps.

1. **Measurement voting** Since we do not assume any prior knowledge about measurement faults, we uniformly initialize the value of  $\gamma_k$  with  $K_t^{-1}$  for all values of  $k \in \{1, \dots, K_t\}$ . The initial value of extended state-space particle weights  $\{w_t^{(i, \chi=k)}\}_{i=1}^N$  is set using the previous time instant weights as

$$w_t^{(i, \chi=k)} = K_t^{-1} \cdot w_{t-1}^{(i)} \quad \forall i \in 1, \dots, N, k \in 1, \dots, K_t. \quad (9)$$

Since the particle weights  $\{w_t^{(i)}\}_{i=1}^N$  and confidence scores  $\{\gamma_k\}_{k=1}^{K_t}$  are interdependent, we cannot obtain a closed form expression for their updated values. Therefore, we introduce a set of random variables  $\{V^k\}_{k=1}^{K_t}$ , referred to as *votes*, to indirectly compute the updates for both particle weights  $\{w_t^{(i)}\}_{i=1}^N$  and confidence scores  $\{\gamma_k\}_{k=1}^{K_t}$ . The vote random variable  $V^k$  denotes the confidence associated with the  $k$ th measurement given a state  $x_t$ . Note that the vote random variable  $V^k$  differs from the confidence score  $\gamma_k$  since it also depends on the state random variable  $x_t$ . Using the initial values of particle weights  $\{w_t^{(i)}\}_{i=1}^N$  and measurement confidence scores  $\{\gamma_k\}_{k=1}^{K_t}$ , we first compute a probability distribution of the vote random variables  $\{V^k\}_{k=1}^{K_t}$ . Then, we use the vote random variables  $\{V^k\}_{k=1}^{K_t}$  to compute the updated value of particle weights  $\{w_t^{(i)}\}_{i=1}^N$  and measurement confidence scores  $\{\gamma_k\}_{k=1}^{K_t}$ . This is analogous to the expectation and maximization steps in the EM algorithm [36], where latent random variables are used to compute indirect updates for the parameters. We model the probability distribution of vote random variables  $\{V^k\}_{k=1}^{K_t}$  as a finite-sample set of votes  $\{v_i^k\}_{i=1, k=1}^{N, K_t}$ , which is computed using the particle distribution  $\tilde{\pi}_t$ . For each particle  $x_t^{(i, \chi)}$  in  $\tilde{\pi}_t$ , we compute a vote  $v_i^k$  for the measurement corresponding to its extended state-space variable  $\chi$  using the normalized residual  $r_i^k$  between the measurement  $\rho_t^k$  and expected measurement  $\hat{\rho}_{x_t^{(i, \chi=k)}}^k$  from particle  $x_t^{(i, \chi=k)}$

$$r_i^k = \frac{\rho_t^{(k)} - \hat{\rho}_{x_t^{(i, \chi=k)}}^k}{\sigma_{x_t^{(i, \chi=k)}}^k}. \quad (10)$$

Next, we compute the vote  $v_i^k$  using the normalized measurement residual  $r_i^k$  from  $i$ th particle to the satellite associated with  $k$ th measurement. In line with traditional residual-based RAIM techniques [8], we leverage the chi-squared distribution with a single degree of freedom (equivalent to the distribution of a squared standard Gaussian random variable [37])

$$v_i^k = P_{\mathcal{N}^2(0,1)}\left(\left(r_i^k\right)^2\right), \quad (11)$$

where  $P_{\mathcal{N}^2(0,1)}(\cdot)$  denotes the probability density function of the square of standard Gaussian distribution [37]. The chi-squared distribution assigns smaller probability value to large residuals than the Gaussian distribution. This is a desirable property in computing the votes, since the difference in the votes computed for different measurements are more evident.

2. **Vote pooling** Next, the votes cast by each particle are normalized and pooled to compute  $\gamma_k$  for each measurement. Similar to the maximization step in the EM algorithm [36], we write an expression for the total empirical probability  $\pi_t^{tot}$  at time  $t$  of measurements  $M_t$  using the votes  $\{v_i^k\}_{i=1, k=1}^{N, K_t}$  and confidence scores  $\{\gamma_k\}_{k=1}^{K_t}$  as

$$\pi_t^{tot} = \sum_{i=1}^N \sum_{k=1}^{K_t} \gamma_k w_t^{(i, \chi=k)} v_i^k. \quad (12)$$

We maximize  $\pi_t^{tot}$  with respect to  $\{\gamma_k\}_{k=1}^{K_t}$  and the constraint  $\sum_{k=1}^{K_t} \gamma_k = 1$  to obtain an update rule for vote pooling

$$\gamma_k = \frac{\sum_{i=1}^N w_t^{(i, \chi=k)} v_i^k}{\sum_{i=1}^N \sum_{k'=1}^{K_t} w_t^{(i, \chi=k')} v_i^{k'}}. \quad (13)$$

This update rule can be seen as assigning an empirical probability to each  $\gamma_k$  according to the weighted votes.

3. **GMM weighting** Using the computed confidence scores  $\{\gamma_k\}_{k=1}^{K_t}$ , we then update the weights of each extended state-space particle. Given a measurement likelihood model, implementing the particle filter on a machine with finite precision of storing floating point numbers may lead to numerical instability. A commonly used way to avoid finite precision errors is by performing the weighing in the log scale, since a larger variation of weights can be represented with the same number of available bits of information [38]. The weights of the multiplicative likelihood model can be converted to a sum of log-likelihoods of individual terms. However, the GMM likelihood cannot be similarly readily distributed:

$$\log L_t(x_t) = \log P(M_t|x_t) = \log \left( \sum_{k=1}^{K_t} \gamma_k \cdot \mathcal{N} \left( \rho_t^{(k)} | \hat{\rho}_{x_t}^k, (\sigma_{x_t}^k)^2 \right) \right). \quad (14)$$

Therefore, we consider an extended state-space that includes the measurement association variable  $\chi$  described in Section II.A. Hence, the likelihood with respect to the extended state-space is rewritten as

$$P(M_t|x_t, \chi = k) = \gamma_k \cdot \mathcal{N} \left( \rho_t^{(k)} | \hat{\rho}_{x_t}^k, (\sigma_{x_t}^k)^2 \right). \quad (15)$$

The measurement likelihood can now be equivalently written as a Categorical distribution likelihood [36]

$$P(M_t|x_t, \chi) = \prod_{k=1}^{K_t} (\gamma_k \cdot \mathcal{N} \left( \rho_t^{(k)} | \hat{\rho}_{x_t}^k, (\sigma_{x_t}^k)^2 \right))^{\mathbb{I}[\chi=k]} \quad \text{s.t.} \quad \sum_{k=1}^{K_t} \gamma_k = 1, \quad (16)$$

where  $\mathbb{I}[\cdot]$  denotes an indicator function which is 1 if the condition in its argument is true and zero otherwise. With this formulation, we take the log of the above expression to obtain the measurement log-likelihood

$$\log L_t(x_t) = \log P(M_t|x_t) = \sum_{k=1}^{K_t} \mathbb{I}[\chi = k] \left( \log \gamma_k + \log \mathcal{N} \left( \rho_t^{(k)} | \hat{\rho}_{x_t}^k, (\sigma_{x_t}^k)^2 \right) \right) \quad \text{s.t.} \quad \sum_{k=1}^{K_t} \gamma_k = 1. \quad (17)$$

We use the log likelihood derived above to compute the new weights  $\{w_t^{(i,\chi=k)}\}_{i=1,k=1}^{N,K_t}$  for each particle in a stable manner

$$l_k^{(i)} = \log L_t(x_t^{(i,\chi=k)}) - \max_i \left( \log L_t(x_t^{(i,\chi=k)}) \right), \quad (18)$$

$$w_t^{(i,\chi=k)} = \frac{\exp \left( l_k^{(i)} \right)}{\sum_{i=1}^N \exp \left( l_k^{(i)} \right)}. \quad (19)$$

#### D. Reduced Resampling Step

Resampling is a commonly used technique in particle filters to avoid the problem of particle degeneracy [19]. It achieves this by redistributing particles such that more particles are present in regions of higher importance. Resampling is typically performed via a sequential importance resampling (SIR) procedure [39], where the weights of particles form a categorical distribution from which new particles are sampled. Many advanced resampling schemes, such as KL Divergence based resampling [40], genetic resampling [18], or resampling using chaos theory [21], have been used in particle filter algorithms for GNSS-based navigation. However, these methods are computationally demanding and hence are not explored in this work.

In Particle RAIM, we use the SIR procedure with a modification, where the  $N \times K_t$  weighted extended state-space particles are reduced to the original number of particles  $N$  with equal weights

$$\{x_t^{(i)}\}_{i=1}^N \leftarrow \text{SIR} \left( \{(x_t^{(i,\chi=k)})\}_{i=1,k=1}^{N,K_t}, w_t^{(i,\chi=k)} \right), \quad (20)$$

where  $\text{SIR}(\cdot)$  is the SIR procedure [39] that resamples from the distribution of weighted extended space particles. The mean state estimate  $\hat{x}_t$  denotes the state solution from the algorithm, and is computed as  $\hat{x}_t = \sum_{i=1}^N w_t^{(i)} x_t^{(i)}$ .

#### E. Integrity Monitoring

A key feature of our IM approach is that we consider a non-Gaussian probability distribution of the receiver state. Our integrity monitor is based on two fundamental assumptions: First, we assume that sufficient redundancy exists in positioning information across the combination of measurements from different satellites and multiple time epochs. Second, we assume that the positions which are likely under faulty measurements have lower correlation with the filter dynamics across time than the positions which are likely under non-faulty measurements.

We develop a Bayesian framework for IM similar to [26]. At each time instant, the integrity monitor calculates measures of integrity risk  $P_I$  and accuracy  $r_A$ , which are derived later in the section. The integrity monitor then compares the integrity risk  $P_I$  and accuracy  $r_A$  against prespecified reference values to detect whether the positioning error between the Particle RAIM state estimate and the ground truth position exceeds a specified alarm limit (AL). Following the Stanford-ESA integrity diagram [41], we refer to such events as hazardous operations. If hazardous operations are detected, the integrity monitor declares the system as unavailable.

**Integrity risk** is defined as the probability that the position error at a time instant is greater than the specified AL. In [26], separate particle filter distributions are tracked for different instances of the measurement fault indicator vector. Hence, integrity risk  $P_I$  in [26] is computed by combining the particle filter probability distributions across different measurement fault indicators

$$P_I \approx \hat{P}_I = 1 - \sum_{j=1}^{2^{K_t}} \frac{1}{2^{K_t}} \sum_{i \in \Omega_j} w_t^{(i,j)}, \quad (21)$$

where

$\hat{P}_I$  is the estimated integrity risk;

$\Omega_j$  denotes the set of particle indices associated with the  $j$ th vector containing fault indicators, such that the particles lie within AL of the mean state estimate  $\hat{x}_t$ ;

$w_t^{(i,j)}$  denotes the  $i$ th particle weight in the set of particles associated with  $j$ th multipath indicator vector at time  $t$ .

The probability of each vector of fault indicators is set uniformly to be  $(2^{K_t})^{-1}$  since we do not assume any prior knowledge about the faults. This formulation assumes that the combined distribution estimated by the particle filters in [26] accurately models the probabilities at tail-ends of the state probability distribution. However, such an assumption might not always hold, since the particle filter algorithm is designed to estimate the probability distribution in the vicinity of the most probable states and not the tail-ends [42]. Therefore, we derive an alternative approach to compute integrity risk directly from our GMM measurement likelihood

$$\begin{aligned}
P_I &= P(\{x_t \notin \Omega_I\} | M_t, u_t, \hat{\pi}_{t-1}) \\
&= 1 - \frac{P(\{x_t \in \Omega_I\} | u_t, \hat{\pi}_{t-1})P(M_t | \{x_t \in \Omega_I\}, u_t, \hat{\pi}_{t-1})}{P(M_t | u_t, \hat{\pi}_{t-1})} \\
&= 1 - \frac{P(\{x_t \in \Omega_I\} | u_t, \hat{\pi}_{t-1})}{P(M_t | u_t, \hat{\pi}_{t-1})} \int_{x_t} P(x_t | \{x_t \in \Omega_I\}, u_t, \hat{\pi}_{t-1})P(M_t | x_t)dx_t \\
&\approx \hat{P}_I = 1 - \frac{P(\{x_t \in \Omega_I\} | u_t, \hat{\pi}_{t-1})}{\pi_t^{tot}} \int_{x_t \in \Omega_I} |\Omega_I|^{-1} \sum_{k=1}^{K_t} \gamma_k \mathcal{N}(\rho_t^{(k)} | \hat{\rho}_{x_t}^k, (\sigma_{x_t}^k)^2) dx_t \quad (22)
\end{aligned}$$

where  $\Omega_I$  denotes the set of positions that lie within AL about the mean state estimate  $\hat{x}_t$  and  $|\Omega_I|$  denotes its total area. For simplicity, we approximate the conditional distribution  $P(x_t | \{x_t \in \Omega_I\}, u_t, \hat{\pi}_{t-1}) \approx |\Omega_I|^{-1} \forall x_t \in \Omega_I$ . We empirically verify that this approximation works well in practice for determining the system availability.

For computational efficiency, we approximate the above integral using cubature techniques for two-dimensional disks described in [43]. The term  $P(\{x_t \in \Omega_I\} | u_t, \hat{\pi}_{t-1})$  is computed by adding the weights of particles that lie inside AL based on the propagated distribution  $\tilde{\pi}_t$ .

**Accuracy** is defined in [26] as the radius of the smallest disk about mean state estimate  $\hat{x}_t$  that contains the actual vehicle state with a prespecified probability  $\alpha$ . Accuracy is determined mainly by the probability mass near the state estimate and not the tail-ends. First, we approximate the particle distribution by a Gaussian distribution with mean as mean state estimate  $\hat{x}_t$ , and covariance  $\mathbf{C}$  computed as a weighted estimate from samples as

$$\mathbf{C} = \frac{1}{1 - \sum_{i=1}^N (w_t^{(i)})^2} \sum_{i=1}^N w_t^{(i)} (x_t^{(i)} - \hat{x}_t)(x_t^{(i)} - \hat{x}_t)^\top. \quad (23)$$

Next, we estimate the accuracy  $r_A$  using the inverse cumulative probability distribution of the approximated Gaussian distribution as

$$r_A \approx \hat{r}_A = \max_{i=1,2} \sqrt{\mathbf{C}_{i,i}} \Phi^{-1}(\alpha) \quad (24)$$

where

$\hat{r}_A$  is the estimated accuracy;

$\Phi^{-1}(\cdot)$  denotes the inverse cumulative probability function for standard Gaussian distribution.

A smaller value of  $r_A$  computed by the expression implies higher accuracy in positioning.

**Availability** is the probability that a positioning solution can be computed by the system with a required integrity risk  $P_I^0$  and accuracy  $r_A^0$ . We determine that our positioning system is available with probability 1 if

$$(\hat{P}_I \leq P_I^0) \quad \text{and} \quad (\hat{r}_A \leq r_A^0). \quad (25)$$

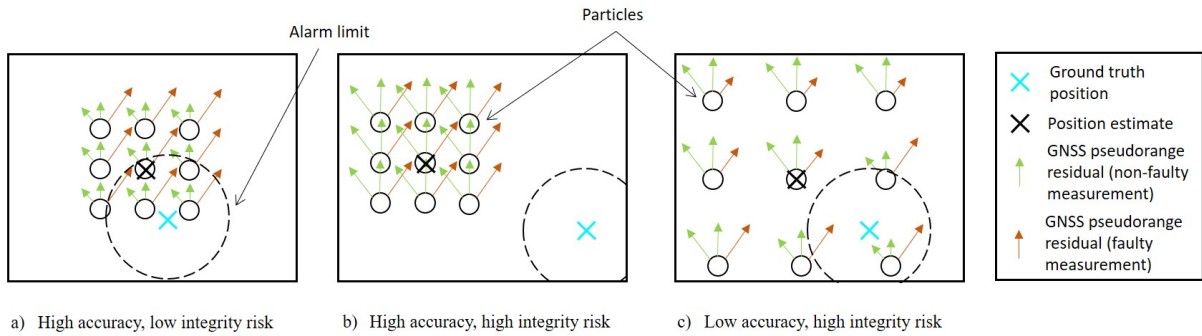


Figure 3: Three typical scenarios encountered by our integrity monitoring algorithm. Each scenario depicts one time instant with three GNSS pseudorange measurements. One out of the three measurements (orange) is contaminated with bias error, and the remaining two measurements (green) are non-faulty. In scenario a), state estimate is within alarm limit and the particles are close to each other (high accuracy, nominal operations). The residuals for non-faulty measurements (green) are smaller than the faulty measurement residuals (orange). Therefore, integrity risk is computed primarily from the GMM components of the non-faulty measurements (high confidence scores) and the system is declared available. In scenario b), state estimate is outside alarm limit and the particles are close to each other (high accuracy, hazardous operations). The residuals for all measurements are large. Therefore, integrity risk is computed from all GMM components (similar confidence scores) and the system is declared unavailable. In scenario c), state estimate is outside alarm limit and the particles are spread apart (low accuracy, hazardous operations). Different parts of the particle distribution have different measurement residuals. Therefore, integrity risk is computed from all GMM components (similar confidence scores) and the system is declared unavailable.

If any of the above constraints are violated, the integrity monitor declares the system unavailable.

Fig. 3 depicts three scenarios to explain the working of our IM algorithm. In the first scenario, Particle RAIM correctly tracks the ground truth trajectory with high accuracy (nominal operations). Among the three measurements obtained for the current time instant, one measurement is contaminated with bias error. In such scenario, Particle RAIM correctly assigns high confidence scores to the non-faulty measurements and a low confidence score to the faulty measurement. Hence, a majority of the probability mass associated with the GMM measurement likelihood constructed from the measurements and confidence scores lies in the vicinity of the state estimate, resulting in small value of the integrity risk. Since the accuracy is high and the integrity risk is low, the integrity monitor correctly declares the system available. In the second scenario, Particle RAIM tracks an incorrect state with high accuracy (hazardous operations). Among the three measurements obtained at the current time instant, two measurements are non-faulty and the remaining third measurement contains a random bias error. In this case, Particle RAIM assigns similar confidence scores to the three measurements, since none of them support the particle distribution. Hence, the probability mass associated with the constructed GMM measurement likelihood lies away from the state estimate, resulting in a large value of the integrity risk. Since the integrity risk is high, the integrity monitor correctly declares the system unavailable. In the third scenario, the particle distribution in Particle RAIM is near the ground truth trajectory, but the particles are spread apart such that the computed accuracy is low (hazardous operations). The three measurements obtained at the current time instant support the positions in the vicinity of different particles. Again, Particle RAIM assigns similar confidence scores to the measurements, since each of them is supported by a different group of particles. Hence, the probability mass associated with the constructed GMM measurement likelihood is spread over a wide range of positions, resulting in a high value of the integrity risk. Since accuracy is low and integrity risk is high, the integrity monitor correctly declares the system unavailable. The third scenario can also result in false alarms by the integrity monitor if the position error in the state estimate computed from the particle distribution happens to be within the alarm limit.

## F. Computation Time

Real-time performance and continuous operation are necessary aspects of a reliable navigation system. However, most existing algorithms based on RAIM of filter-bank approaches exhibit large computation overheads when more than a few (one or two) measurement faults are considered. For example, in solution-separation RAIM [5] and filter-bank approaches [18], different hypotheses associated with certain measurements being faulty need to be considered. For maximum  $m$  faults considered within  $k$  available measurements, the number of such hypotheses roughly grows on the order of  $O(k^m)$ .

Instead, the multiple fault mitigation scheme in Particle RAIM grows linearly in computation with the number of available measurements. For  $n$  particles and  $k$  available measurements, both the vote computation and vote pooling have a complexity of  $O(nk)$ . Constructing the GMM likelihood from confidence scores requires  $O(k)$  computations. Finally, computing weights for each extended space particle requires  $O(nk)$  computations. All these operations together exhibit a computational complexity of at most  $O(nk)$ , or linear in  $k$  for a fixed  $n$ . Furthermore, each of these steps admits parallelization. For example, all votes from particles to measurements can be computed in parallel and pooling of votes can be performed at the same time across different measurements. Additionally, weights for all the particles can be computed simultaneously from the likelihood model, resulting in further speedups. However, the number of particles required to adequately approximate the probability distribution increase exponentially with the size of the state-space [19]. In order to maintain a small computation cost with large state-spaces, more complex strategies, such as Rao-Blackwellization [44] or leveraging prior knowledge about probability distribution, need to be employed.

## III. Experimentation Results

We evaluated the framework for localization performance and IM on both simulated as well as real-world driving scenarios. For the experiments on simulated data, we validated our algorithm across multiple runs on various simulated noise profiles that imitate GNSS measurements in urban environments.

We consider two baselines to compare against our Particle RAIM algorithm:

**Joint state-space particle filter (J-PF)** For our first baseline, we consider the particle filter algorithm proposed by Pesonen [26] which considers both the vehicle navigation parameters and measurement fault vector (signal quality parameters) in the particle filter state-space. The combined state-space is referred to as the *joint state-space*. J-PF requires considering separate particles for each binary-valued vector denoting faulty measurements, resulting in a combinatorial growth in computational complexity on increasing number of considered faults. For example, when only 1 fault is considered in 10 available measurements, the different sets of particles considered by the algorithm is 10, each associated with the fault being present in one of the 10 measurements. When the number of faults is increased to 2, all the pairs of measurements need to be considered increasing the number of particle sets to 55 (both single and double faults). With 3 faults, this number further increases to 175. Therefore, we limit the number of faults considered in GNSS measurements for J-PF to at most 2 for computational tractability. The particle filter approach described in [26] also assumes a transition model for fault indicators across time instants. To compare against our approach which does not assume a transition model for fault indicators, we set the fault indicator transitions in J-PF to be equally probable from the most likely (highest log likelihood) fault indicator vector at the current time instant to any other vector. For all the fault indicator vectors that are not the most likely, we set the transitions to any other vector as zero. This approach is also in line with the Rao-Blackwellized particle filter discussed in the same paper [26] as well as filter bank approaches [45], where the filter distribution with the highest log-likelihood is selected to represent the probability distribution at a time instant. However, we only use the highest log-likelihood probability distribution for transitions and computation of state estimate, while all the particles are used for determining the system availability in IM.

**Kalman filter RAIM (KF-RAIM)** Our second baseline is the residual-based RAIM algorithm [8] combined with Kalman filter for sequential state estimation. Similar to the strategy used in [46], we iteratively detect measurement faults using the chi-square test statistic computed from the Kalman filter state estimate. In each iteration, the measurement with the largest residual is removed and the Kalman filter measurement update step is performed.

The process of detecting and excluding measurement faults is repeated till the test statistic falls below a specified threshold. The detection threshold is computed from the inverse chi-squared distribution and a false alarm requirement, which we empirically set to  $10^{-7}$ . We monitor the integrity in KF-RAIM using the sequence of normalized Kalman filter innovations [16] computed within 10 s long time windows for simplicity.

All the filters are initialized at the ground truth initial position with a specified standard deviation  $\sigma_{init}$ . Note that for Particle RAIM, we only used a single iteration in the weighting step in our experiments on simulated data, since we observed that a single iteration suffices to provide us good performance at low computation cost.

**Localization Performance Metrics** For evaluating the positioning performance of our approach, we compute the metrics of horizontal root mean square error (RMSE) as well as the percentage of estimates that deviate more than 15 m from the ground truth ( $\%>15$  m). We compute these metrics as

$$RMSE = \sqrt{\frac{1}{T} \sum_{t=1}^T \|\hat{x}_t - x_t^*\|_{\text{pos}}^2}, \quad (26)$$

$$\%>15 \text{ m} = \frac{N(\|\hat{x}_t - x_t^*\| > 15)}{T}, \quad (27)$$

where

$T$  denotes the total number of timesteps for which the algorithm is run;

$x_t^*$  denotes the ground truth state of the receiver;

$\|x\|_{\text{pos}}$  denotes the Euclidean norm of the horizontal position coordinates in state  $x$ ;

$N(I)$  denotes the number of occurrences of event  $I$ .

**Integrity Monitoring Performance Metrics** We evaluate the performance of our integrity monitor on its capability to raise alarms (declare system unavailable) when the navigation system is under hazardous operations. In our experiments, we declare hazardous operations as the event when the positioning error in the navigation system exceeds an alarm limit, which we set to 20 m. We evaluate the integrity monitor on the metrics of estimated probability of false alarm  $\hat{P}(FA)$  and probability of missed-identification  $\hat{P}(MI)$  in determining the system availability. These metrics are computed as

$$\hat{P}(FA) = \frac{N(I_{av} \cap \neg I_{ho})}{N(\neg I_{ho})}, \quad (28)$$

$$\hat{P}(MI) = \frac{N(\neg I_{av} \cap I_{ho})}{N(I_{ho})}, \quad (29)$$

where

$I_{av}(\neg I_{av})$  denotes the event when the navigation system is declared available (unavailable) by the IM algorithm;

$I_{ho}(\neg I_{ho})$  denotes the event of hazardous operations (normal operations).

The rest of the section is organized as follows: (A) evaluation of Particle RAIM localization performance on simulated data and comparison with KF-RAIM and J-PF approaches, (B) evaluation of Particle RAIM on real-world data, (C) comparison of our IM technique with Bayesian RAIM [26] and Kalman filter innovation sequence [16] on simulated scenarios, (D) analysis of the computation time of our algorithm and comparison in terms of computation with KF-RAIM and J-PF approaches, and (E) discussion of the results.

Parameter	Value
# of satellites	5-10
GNSS ranging noise $\sigma_{GNSS}$	5-10 m
GNSS ranging bias error magnitude	50-200 m
Maximum # of faulty measurements	1-6
GNSS fault change probability	0.2
Vehicle speed	10 m/s
Odometry noise $\sigma_u$	5 m/s
# of particles	200
Filter initialization $\sigma_{init}$	5 m
Filter measurement model noise $\{\sigma^k\}_{k=1}^K$	5 m
Filter propagation model noise $\sigma_f$	5 m
Alarm limit $AL$	20 m
Accuracy probability requirement $\alpha$	0.5

Table 2: Experimental parameters for simulated scenario

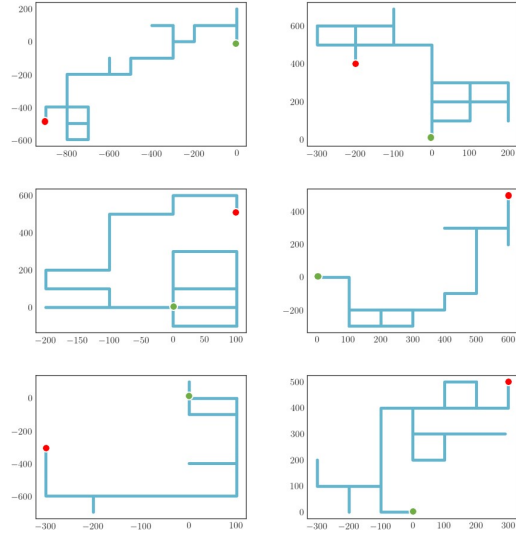


Figure 4: Sample trajectories (cyan) from randomly generated simulation dataset. The start and end points of the trajectories are drawn in green and red respectively. Each trajectory is approximately 4000 m long and of duration 400 s.

### A. Evaluation on simulated scenarios

We evaluated our approach on multiple simulated driving scenarios with varying noise profiles in GNSS and odometry measurements. Our choice of simulations is motivated by two factors: accurate ground truth information is available and multiple measurement sequences with different noise values can be obtained. Our simulation environment consists of a vehicle moving on the horizontal surface according to 50 different randomly generated trajectories approximately of length 4000 m each (Fig. 4). The vehicle obtains noisy GNSS ranging measurements from multiple simulated satellites as well as noisy odometry measurements. The simulated satellites move with a constant velocity of 1000 m/s along well-separated paths in random directions at fixed heights of  $2 \times 10^7$  m from the horizontal surface. The odometry consists of vehicle speed measurements, and an accurate heading direction of the vehicle is assumed to be known (eg. from a high accuracy magnetometer). A driving scenario lasts for 400 s with measurements acquired at the rate of 1 Hz. In each state estimation algorithm, we track the 2D state  $(x, y)$  of the vehicle. We limit ourselves to the simple 2D case in simulation scenarios in view of the computational overhead from requiring significantly more particles in larger state-spaces. The parameters used for the simulation and filter are given in Table 2.

We induce two kinds of noise profiles in our pseudorange measurements from the simulation - a zero mean Gaussian random noise on all measurements and a random bias noise on a subset of measurements. The subset of measurements containing the bias noise is initialized randomly, and has a small probability of changing to a different random subset at every subsequent time instant. The number of affected measurements is selected randomly between zero and a selected maximum number of faults at every change. The zero mean Gaussian noise is applied to measurements such that the variance is double the normal value for biased measurements. Using our noise model, we simulate the effects of NLOS signals and multipath on pseudorange measurements in urban GNSS navigation.

**Localization performance** In this experiment, we vary the number of available and faulty GNSS measurements at a time instant. We compare the localization performance of our algorithm with that of J-PF and SR-RAIM approaches. We consider the following scenarios (total # of measurements, max # of faults): (5, 1), (5, 2), (7, 3), (7, 4), (10, 5), (10, 6). For each of these scenarios, we induce a bias error of 100 m with a standard deviation of 5

		Few-fault scenarios			Many-fault scenarios		
		(5, 1)	(5, 2)	(7, 3)	(7, 4)	(10, 5)	(10, 6)
KF-RAIM	RMSE(m)	7.6	21.5	22.0	34.3	25.5	34.4
	%>15 m	5.9	68.7	69.6	87.4	80.5	91.1
J-PF	RMSE(m)	<b>4.8</b>	<b>5.8</b>	28.1	33.5	25.6	22.9
	%>15 m	<b>1.2</b>	<b>3.1</b>	79.0	94.2	68.3	85.4
Particle RAIM	RMSE(m)	11.0	12.4	<b>11.7</b>	<b>13.2</b>	<b>12.2</b>	<b>12.4</b>
	%>15 m	23.4	26.6	<b>27.4</b>	<b>33.1</b>	<b>24.3</b>	<b>28.7</b>

Table 3: Comparison of localization performance on the simulated dataset. The dataset consists of varying total number of measurements and maximum number of measurement faults (total # of measurements, max # of faults). Particle RAIM demonstrates better localization performance in scenarios with large number of faults in comparison to J-PF and KF-RAIM.

m in the GNSS measurements. We compute the localization metrics for 50 full runs of duration 400 s each across different randomly generated trajectories.

The trajectories for two scenarios, (5, 1) and (10, 5), are visualized for each algorithm in Fig. 5 and the computed metrics are recorded in Table 3. As can be seen from the qualitative and quantitative results, Particle RAIM demonstrates better localization performance than the compared approaches for scenarios with high noise degradation while maintaining a low rate of large positioning errors. J-PF has better performance than its counterparts in scenarios with single faults due to considering all possibilities of faults explicitly. However, its performance worsens in scenarios with more than 2 measurement faults. Similarly, KF-RAIM is able to identify and remove faults in scenarios with few faulty measurements resulting in lower positioning errors, but has poor performance in many-fault scenarios.

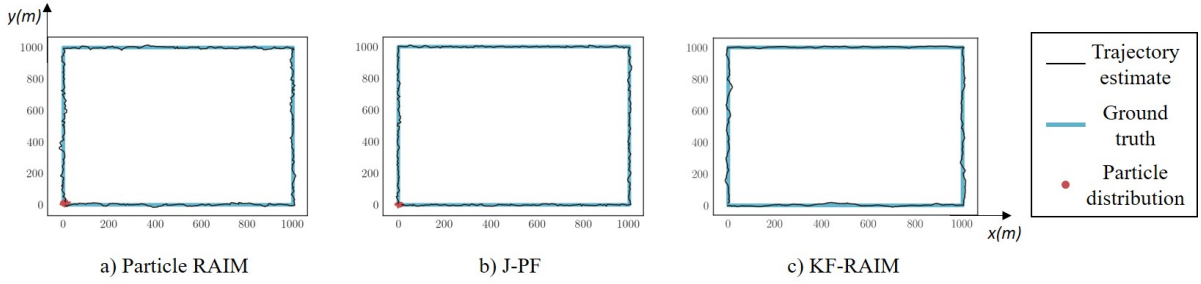
**Varying GNSS measurement noise** In this experiment, we study the impact of GNSS measurement noise bias and standard deviation values on the performance of our algorithm. First, keeping the GNSS measurement standard deviation fixed at 5 m, we vary the bias between 10 – 100 m in increments of 10 m. Next, keeping the bias fixed at 100 m, we vary the standard deviation between 5 – 25 m in increments of 5 m. For all cases, the total number of measurements is kept at 7 and the maximum number of faults is 3. The RMSE for both studies are computed across 20 different runs and plotted in Fig. 6.

The first plot shows that the localization performance of Particle RAIM initially deteriorates and then starts improving. This is because for low bias error values, the faulty GNSS measurements do not have a significant impact on the localization solution, even if the algorithm fails to remove them. Beyond the bias error value of 50 m, the algorithm successfully assigns lower confidence scores to faulty measurements, resulting in lower RMSE for higher bias error values.

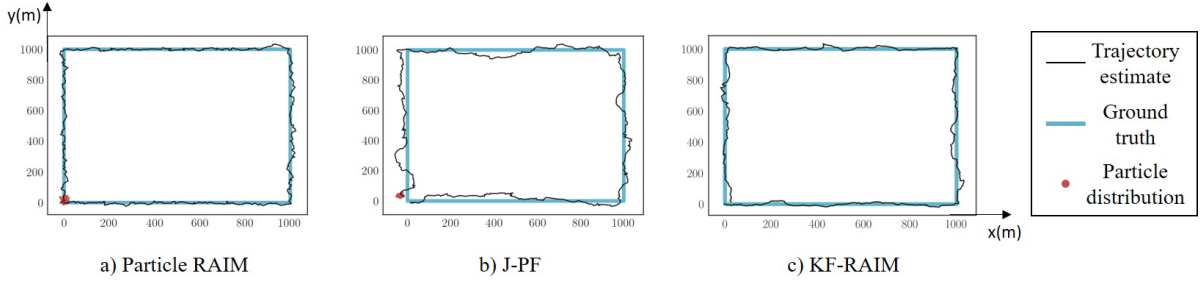
The second plot demonstrates the impact of high measurement noise standard deviation on our approach. As the measurement noise standard deviation is increased, the RMSE increases in a superlinear fashion. The performance deteriorates with increasing noise standard deviation since both the tasks of fault mitigation as well as localization are negatively impacted by an increased measurement noise.

## B. Evaluation on real-world data

For the real-world case, we use GNSS pseudorange and odometry measurements from the publicly available urban GNSS dataset collected by TU Chemnitz for the SmartLoc project [47]. We consider the Frankfurt Westend-Tower trajectory from the dataset for evaluating our approach. The trajectory is  $\sim 2300$  m long and has both dense and sparse urban regions, with 32% of total measurements as NLOS signals.



(a) 1 faulty GNSS measurement out of 5 in total.



(b) 5 faulty GNSS measurements out of 10 in total.

Figure 5: Localization accuracy comparison between Particle RAIM, J-PF, and KF-RAIM approaches for (a) few-fault scenario and (b) many-fault scenario. We fix the underlying ground truth trajectory to be a square of side 1000 m with  $(0, 0)$  as both the start and end positions. Unlike J-PF and KF-RAIM, Particle RAIM is able to estimate the vehicle state with good accuracy in scenarios with a large fraction of faulty measurements.

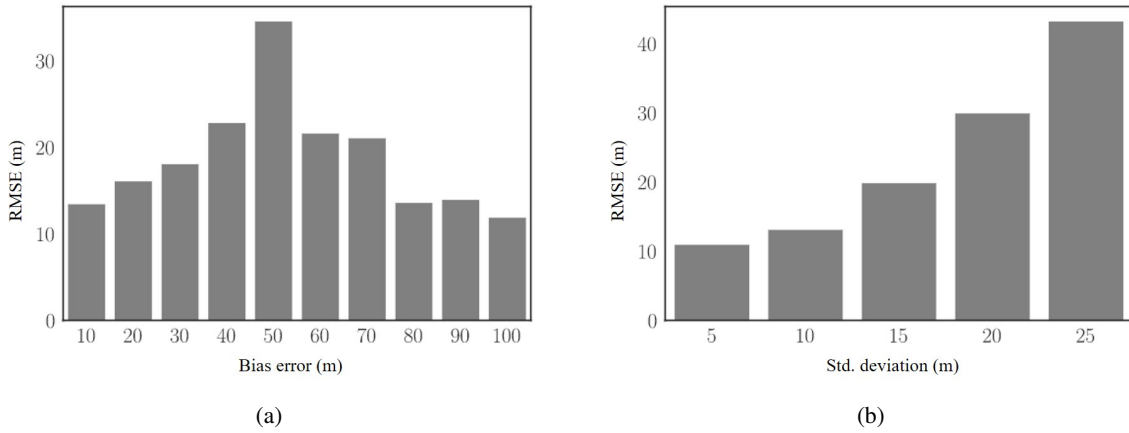


Figure 6: Sensitivity analysis of Particle RAIM localization performance with varying values of GNSS measurements (a) bias and (b) standard deviation. For low values of bias, the faults do not significantly impact the navigation solution, resulting in low RMSE values. Beyond the value of 50 m, Particle RAIM is able to remove the impact of faulty measurements resulting in low RMSE values. The performance of the algorithm increasingly deteriorates with higher standard deviation in GNSS measurement noise since both the capability to remove faulty measurements as well as localization are hampered by an increased noise.

The dataset was collected on a vehicle moving in urban environments, using a low-cost u-blox EVK-M8T GNSS receiver at 5 Hz and CAN data for odometry at 50 Hz. The odometry data contains both velocity and yaw-rate measurements from the vehicle CAN bus. The ground truth or reference position is provided using a high-cost NovAtel GNSS receiver at 20 Hz. Additionally, corrections to satellite ephemeris data are also provided as an SP3

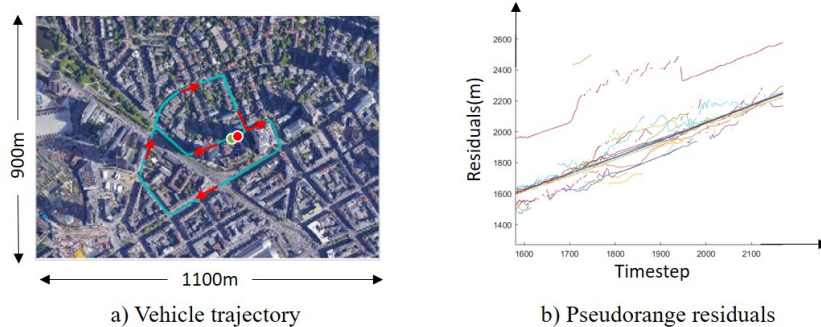


Figure 7: Real-world dataset for validation of our approach. We use Frankfurt Westend-Tower sequence from smartLoc project dataset collected by TU Chemnitz [47]. The trajectory followed by the vehicle is shown in a). The vehicle moves from the start point (green) to end point (red) along the trajectory (cyan) in the direction specified by red arrows. b) shows a plot of pseudorange measurement residuals from different satellites with respect to ground truth position. The residuals were selected from a dense urban region in the dataset for a duration of 2 minutes. Clock differences across different GNSS constellations were removed by subtracting measurement residuals from initial vehicle position. Multiple pseudorange measurement residuals demonstrate errors due to multipath effects in the urban environment.

file along with the data.

The receiver collects  $\sim 12$  pseudorange measurements at each time instant from GPS, GLONASS, and Galileo constellations. As a preprocessing step, we subtract the measurement residuals corresponding to the initial vehicle state from all measurements. This is done to remove inter-constellation clock error differences as well as assign zero residuals to all GNSS measurements at the initial vehicle position. Fig. 7 shows the reference trajectory used for evaluation as well as measurement residuals with respect to ground truth position in a dense urban region for a duration of 2 minutes.

Our state-space consists of the vehicle position  $(x, y)$ , heading  $\theta$ , and clock bias error  $\delta t$ . To mitigate the impact of clock drift, we denote clock bias error  $\delta t$  as the difference between the true receiver clock bias and a simple linear drift model with precomputed drift rate, and estimate this difference across time instants. We do not track the clock drift to keep the state size small for computational tractability. Note that in practice, the clock parameters can be determined separately using least-squares while the positioning parameters can be tracked by our approach for efficient computation. For Particle RAIM and J-PF, we use 1000 particles to account for a larger state space size than the simulated scenario. Additionally, we use 5 iterations of weighting in Particle RAIM, which is empirically determined to achieve small positioning errors on the scenario.

Fig. 8 shows the position estimates from Particle RAIM, J-PF, and KF-RAIM. Particle RAIM position estimates are closer to the ground truth than compared approaches and thereby have lower horizontal RMSE values. J-PF and KF-RAIM achieve similar RMSE values and visually exhibit a higher variance in state estimation error than Particle RAIM.

### C. Comparison of integrity monitoring approaches

We study the IM performance of Particle RAIM on simulated and real-world data. Since obtaining a large amount of real-world data is difficult and out of scope for this work, we restrict our numerical analysis to simulated data and only provide qualitative results on real-world data. For the simulated scenario, we generate 400 s long trajectories with GNSS pseudorange measurements acquired at the rate of 1 Hz (Fig. 9 a)). GNSS pseudorange measurements are simulated from 10 different satellites. At time instants between 125-175 s, we add bias errors in upto 60% of the available measurements, such that the faulty measurements correspond to a position offset from the ground truth position. The position offset is randomly selected across different runs from between 50 – 150 m. To limit our analysis to GNSS measurements, we do not simulate any odometry measurements for the simulations

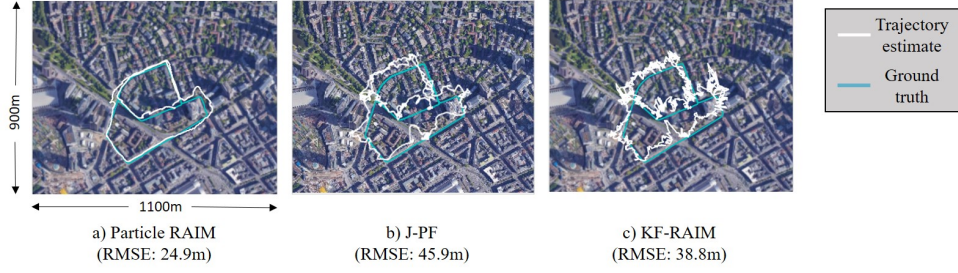


Figure 8: Estimated trajectories on real-world data. Particle RAIM (a) produces a closer trajectory to ground truth as compared to trajectory from J-PF (b) and KF-RAIM (c). The horizontal RMSE values are computed by averaging over 20 runs with different randomness values in initialization and propagation. In regions where multiple measurements contaminated with bias errors, Particle RAIM (a) is able to localize better than the baselines by assigning high confidence scores to measurements that are consistent with the particle filter probability distribution of vehicle state.

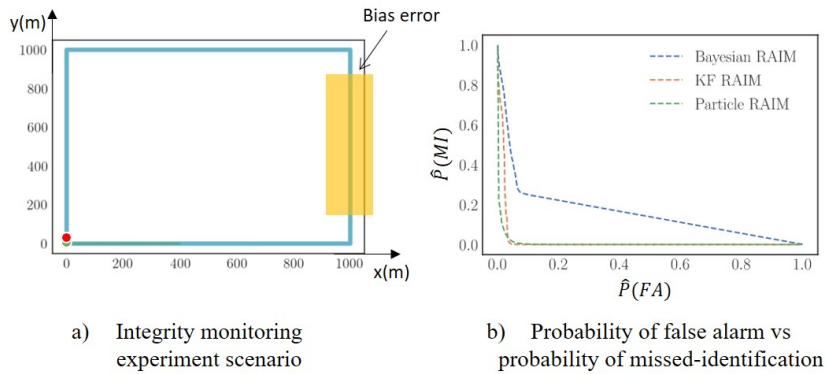


Figure 9: (a) Simulation experiment scenario for analyzing integrity monitoring performance. The start and end of the 400 s long trajectory are marked in green and red, respectively. The yellow region denotes the 125 – 175 s positions in the trajectory, when bias errors are induced in upto 60% of the total 10 simulated GNSS measurements. (b) Probability of false alarms and probability of missed-identifications across different integrity monitoring threshold values for Particle RAIM, Bayesian RAIM [26], and innovation sequence in KF RAIM [16] computed from more than  $10^4$  samples across multiple runs. Particle RAIM generates lower false alarms and missed-identifications than Bayesian RAIM across all thresholds, and demonstrates a comparable performance to KF-RAIM.

and localize only using GNSS pseudorange measurements for all the filters. For the particle filter algorithms, we set the propagation noise standard deviation to 20 m to ensure that the position can be tracked in the absence of odometry measurements.

The IM algorithms in all 3 considered approaches depend on different threshold values. In Particle RAIM and Bayesian RAIM, a reference value of minimum accuracy and integrity risk is required. In Kalman filter innovation-based approach, a threshold for the innovation statistic needs to be computed from the integrity requirements. Varying the threshold values results in a trade-off between  $\hat{P}(FA)$  and  $\hat{P}(MI)$ . For example, setting the threshold such that an alarm is always generated produces many false alarms, but no missed-identifications. Alternatively, setting the threshold to not generate any alarms produces no false alarms but many missed identifications. Therefore, we compare the IM performance by computing  $\hat{P}(FA)$  and  $\hat{P}(MI)$  across different values of the thresholds and visualizing the trade-off (Fig. 9 b)). All the metrics are calculated using more than  $10^4$  samples across multiple runs of the simulation for each algorithm. Fig. 9 b) shows that Particle RAIM generates lower false alarms and missed-identifications than Bayesian RAIM across different threshold values. Furthermore, the performance of our approach is comparable to the Kalman filter innovation sequence method in KF-RAIM on the simulation

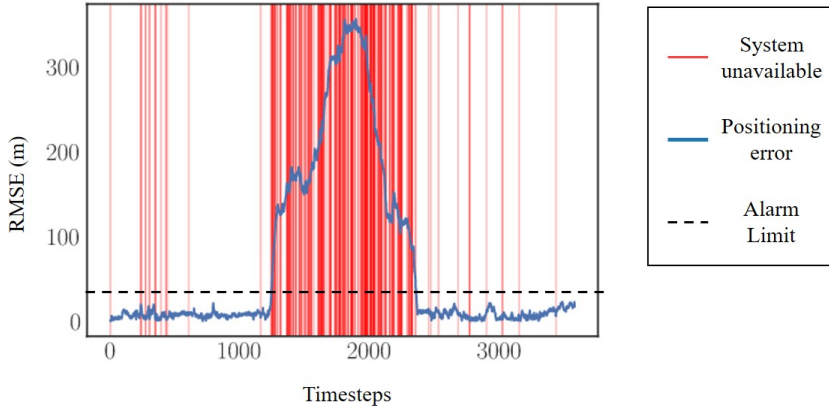


Figure 10: Particle RAIM system availability on a randomly selected run on the real-world driving scenario. Our IM algorithm is able to correctly declare the system as unavailable in most events when the positioning error exceeds the alarm limit.

scenario.

For qualitative analysis, we plot the RMSE and Particle RAIM system availability for a trajectory with large positioning errors on the real-world driving scenario (Fig. 10). The integrity risk and accuracy thresholds (set as 0.45 and 7 m, respectively) for the scenario are manually selected to minimize missed-identifications while maintaining high availability. As can be seen in the figure, Particle RAIM declares the system unavailable in most cases when positioning error exceeds the alarm limit. The algorithm also generates false alarms when the state estimation algorithm is unable to establish the reliability of the position estimate from the measurements.

#### D. Analysis of computation time

We compare the computational performance of Particle RAIM, J-PF and KF-RAIM approaches. The average time per timestep in milliseconds is shown in Fig. 11. For Particle RAIM and J-PF approaches, we consider 1000 particles in the particle filter. In Particle RAIM, we apply a single iteration for computing confidence scores. The methods are compared for a scenario with 10 total measurements and 6 faults. Particle RAIM requires less than half of the computation time required by J-PF, which only considers upto 2 faults. KF-RAIM exhibits the least computation time since the updates are calculated analytically instead of using particles. Table 4 contains the fractions of total computation time taken up by different components of the Particle RAIM algorithm. The maximum fraction of the computation time is taken by the Measurement Voting and Mixture Weighting steps, since they require accessing each particle as well as measurement and performing multiple operations on them. The benchmarking is done on a laptop computer with Intel i7-9750H x64-based processor with 16 Gigabytes of RAM and a 6 core 2.60 GHz CPU.

#### E. Discussion

Our results for state estimation performance on simulated and real driving scenarios show that Particle RAIM achieves lower horizontal positioning errors compared to J-PF and KF-RAIM. This is because unlike J-PF which is limited by computation to 2 measurement faults, Particle RAIM mitigates multiple measurement faults using the iterative weighting process. Furthermore, Particle RAIM incorporates measurement residuals from multiple particles for fault mitigation unlike KF-RAIM, which relies on post-measurement update residuals from the state estimate.

Our evaluation of IM approaches on multiple simulation runs demonstrates that Particle RAIM attains fewer false alarms and missed identifications across threshold values in determining the system availability compared to Bayesian RAIM and comparable performance to the Kalman filter innovation sequence technique. However,

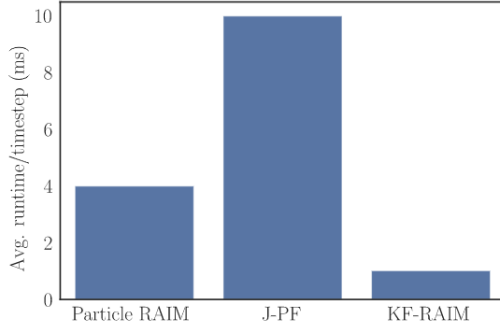


Figure 11: Comparison of computation times in Particle RAIM, J-PF and KF-RAIM. We use 1000 particles in Particle RAIM and J-PF. Particle RAIM requires lower computation time than J-PF due to its linear-time complexity algorithm. KF-RAIM requires the least computation time since the updates are calculated analytically instead of using particles.

Component	Compute[%]
Propagation	0.35
Measurement Voting	49.55
Vote Pooling	0.29
Mixture Weighting	49.28
Resampling	0.53

Table 4: Component-wise fractions of total computation time in Particle RAIM. Measurement voting and Mixture weighting are the most computation-heavy components in the algorithm, since they involve multiple operations across all particles and measurements.

a drawback of our approach over the innovation sequence integrity monitor is that it currently lacks theoretical guarantees of performance under simplified measurement noise assumptions. Nevertheless, our results suggest that our approach is a promising direction for future research on detecting hazardous operations in urban environments.

Our analysis of the computational performance of our approach shows that Particle RAIM requires less than half the runtime required by J-PF and can therefore be deployed in real-time. This is because unlike J-PF which considers multiple subsets of measurements, Particle RAIM mitigates measurement faults using a single set of extended state-space particles. However, Particle RAIM requires  $\sim 4\times$  more computation time than KF-RAIM, which uses analytically derived expressions for fault mitigation and state estimation instead of particles.

Although Particle RAIM achieves good localization performance in simulated scenarios with multiple faulty measurements, the algorithm’s performance in scenarios with one or two measurement faults is worse than J-PF. This is because the algorithm is designed with conservative choices, such as the GMM measurement likelihood model instead of the commonly used multivariate Gaussian model. However, the conservative design of our approach is necessary for robust state estimation in challenging urban scenarios with multiple faults.

Another conservative decision choice is computing the integrity risk by numerically integrating the GMM measurement likelihood. Since the GMM assigns high probability to multiple states which have small residuals for some measurements, the algorithm often generates false alarms even when the filter state estimate is within the alarm limit. Therefore, an avenue for future research is to consider measurement likelihood models other than the GMM likelihood which are less conservative and yet ensure safe and robust navigation in urban environments.

A limitation of our approach is that the fault mitigation strategy in Particle RAIM uses an approximated predicted probability distribution from the previous timestep for computing measurement residuals. Therefore, in scenarios where the probability distribution tracked by the particles significantly differs from the true posterior probability distribution, the algorithm might compute incorrect confidence scores that might cause the filter to diverge in extreme scenarios. Resetting strategies for the filter might help in maintaining good performance in such scenarios. However, analysis of such techniques is out of scope for this paper and left for future research.

Although Particle RAIM achieves competitive performance to existing state estimation and IM algorithms in scenarios with multiple measurement faults, the performance of our algorithm is limited by the precision of GNSS pseudorange and odometry measurements under nominal operations in urban environments. Therefore, an im-

portant future direction for ensuring safe urban navigation is to explore additional sensor modalities with higher precision in positioning, such as carrier phase or camera and LiDAR sensors. In theory, higher precision in localization coupled with larger number of particles improves the performance of the integrity monitor, since integrity risk and accuracy can be computed more accurately for smaller alarm limits. However, this is limited by the computational requirements for a large number of particles.

The number of particles used for approximating the state probability distribution is an important parameter in Particle RAIM that depends on the size of the state-space and on the resolution required in state estimation. On increasing the size of the state space, the number of particles required to approximate the posterior probability distribution increases exponentially [19]. Since the maximum achievable resolution is limited by the precision in GNSS and odometry measurements, we observe no significant improvement in our state estimation experiment results when the number of particles is increased beyond 100 in the simulated scenario and beyond 1000 in the real scenario. In IM, we observe a decrease in the variance of our estimates of integrity risk and accuracy. However, since the system availability depends on comparing integrity risk and accuracy against a threshold, we do not observe a significant decrease in  $\hat{P}(FA)$  and  $\hat{P}(MI)$  when more than 100 particles are used.

Another important parameter in Particle RAIM is the choice of threshold values for accuracy and integrity risk. Varying the thresholds results in different trade-offs between false-alarms and missed identifications. For our experiments, we have compared the algorithms independently of the threshold by analyzing the trade-off between false alarms and missed identifications achieved when the thresholds are varied. However, practical settings currently require the thresholds to be set empirically based on the filter parameters and integrity requirements. Future research will explore setting the thresholds automatically from integrity requirements.

## IV. Conclusion

In this paper, we presented Particle RAIM as a novel probabilistic framework for robust localization and IM in challenging urban environments. Particle RAIM leverages GNSS and odometry measurements to compute a fault-robust probability distribution of the position and raises alarms if a reliable position cannot be estimated. We employ a particle filter for state estimation and developed a GMM measurement likelihood for robustly computing the particle weights. Our approach jointly determines the GMM weight coefficients and particle weights using an iterative algorithm based on EM. To determine the system availability, we compute measures of integrity risk and accuracy and compare them against prespecified reference values. Through a series of experiments on challenging simulated and real-world urban driving scenarios, we have shown that Particle RAIM achieves lower positioning errors in state estimation as well as small probability of false alarm and probability of missed-identification in IM when compared to existing approaches. Furthermore, our approach is capable of mitigating multiple measurement faults with lower computation requirements than existing particle filter-based approaches. Hence, Particle RAIM offers a promising direction for real-time deployment of high-integrity algorithms in urban environments.

## Acknowledgements

This material is based upon work supported by the National Science Foundation under award #2006162.

## References

- [1] N. Zhu, J. Marais, D. Betaille, and M. Berbineau, "GNSS Position Integrity in Urban Environments: A Review of Literature," *IEEE Transactions on Intelligent Transportation Systems*, vol. 19, pp. 2762–2778, Sept. 2018.
- [2] S. Pullen, T. Walter, and P. Enge, "SBAS and GBAS Integrity for Non-Aviation Users: Moving Away from" Specific Risk,"
- [3] B. W. Parkinson, P. Enge, P. Axelrad, and J. J. Spilker Jr, *Global positioning system: Theory and applications, Volume II*. American Institute of Aeronautics and Astronautics, 1996.
- [4] M. Joerges, F.-C. Chan, and B. Pervan, "Solution Separation Versus Residual-Based RAIM," *Navigation*, vol. 61, pp. 273–291, Dec. 2014.
- [5] R. G. Brown and P. W. McBURNEY, "Self-Contained GPS Integrity Check Using Maximum Solution Separation," *Navigation*, vol. 35, pp. 41–53, Mar. 1988.

- [6] Y. C. Lee and others, "Analysis of range and position comparison methods as a means to provide GPS integrity in the user receiver," in *Proceedings of the 42nd Annual Meeting of the Institute of Navigation*, pp. 1–4, Citeseer, 1986.
- [7] M. Joerger and B. Pervan, "Solution separation and Chi-Squared RAIM for fault detection and exclusion," in *2014 IEEE/ION Position, Location and Navigation Symposium-PLANS 2014*, pp. 294–307, IEEE, 2014.
- [8] B. W. Parkinson and P. Axelrad, "Autonomous GPS Integrity Monitoring Using the Pseudorange Residual," *Navigation*, vol. 35, pp. 255–274, June 1988.
- [9] M. A. Sturza, "Navigation System Integrity Monitoring Using Redundant Measurements," *Navigation*, vol. 35, pp. 483–501, Dec. 1988.
- [10] M. Joerger and B. Pervan, "Sequential residual-based RAIM," in *Proceedings of the 23rd international technical meeting of the satellite division of the institute of navigation (ION GNSS 2010)*, pp. 3167–3180, 2010.
- [11] J. Blanch, T. Walter, P. Enge, Y. Lee, B. Pervan, M. Rippl, and A. Spletter, "Advanced RAIM user algorithm description: integrity support message processing, fault detection, exclusion, and protection level calculation," in *Proceedings of the 25th International Technical Meeting of The Satellite Division of the Institute of Navigation (ION GNSS 2012)*, pp. 2828–2849, 2012.
- [12] S. Wallner, "A Proposal for Multi-Constellation Advanced RAIM for Vertical Guidance,"
- [13] A. Grosch, O. Garcia Crespiello, I. Martini, and C. Gunther, "Snapshot residual and Kalman Filter based fault detection and exclusion schemes for robust railway navigation," in *2017 European Navigation Conference (ENC)*, (Lausanne, Switzerland), pp. 36–47, IEEE, May 2017.
- [14] S. Hewitson and J. Wang, "Extended Receiver Autonomous Integrity Monitoring (eRAIM) for GNSS/INS Integration," *Journal of Surveying Engineering*, vol. 136, pp. 13–22, Feb. 2010.
- [15] Z. Li, D. Song, F. Niu, and C. Xu, "RAIM algorithm based on robust extended Kalman particle filter and smoothed residual," in *Lect. Notes Electr. Eng.*, 2017. ISSN: 18761119.
- [16] C. Tanil, S. Khanafseh, M. Joerger, and B. Pervan, "Sequential Integrity Monitoring for Kalman Filter Innovations-based Detectors," (Miami, Florida), pp. 2440–2455, Oct. 2018.
- [17] C. Boucher, A. Lahrech, and J.-C. Noyer, "Non-linear filtering for land vehicle navigation with GPS outage," in *2004 IEEE International Conference on Systems, Man and Cybernetics (IEEE Cat. No.04CH37583)*, vol. 2, (The Hague, Netherlands), pp. 1321–1325, IEEE, 2004.
- [18] E. Wang, T. Pang, Z. Zhang, and P. Qu, "GPS Receiver Autonomous Integrity Monitoring Algorithm Based on Improved Particle Filter," *Journal of Computers*, vol. 9, pp. 2066–2074, Sept. 2014.
- [19] A. Doucet and A. M. Johansen, "A tutorial on particle filtering and smoothing: Fifteen years later," *Handbook of nonlinear filtering*, vol. 12, no. 656-704, p. 3, 2009.
- [20] J.-S. Ahn, R. Rosihan, D.-H. Won, Y.-J. Lee, G.-W. Nam, M.-B. Heo, and S.-K. Sung, "GPS Integrity Monitoring Method Using Auxiliary Nonlinear Filters with Log Likelihood Ratio Test Approach," *Journal of Electrical Engineering and Technology*, vol. 6, pp. 563–572, July 2011.
- [21] E. Wang, C. Jia, G. Tong, P. Qu, X. Lan, and T. Pang, "Fault detection and isolation in GPS receiver autonomous integrity monitoring based on chaos particle swarm optimization-particle filter algorithm," *Adv. Sp. Res.*, 2018.
- [22] J. Blanch, K. Gunning, T. Walter, L. De Groot, and L. Norman, "Reducing Computational Load in Solution Separation for Kalman Filters and an Application to PPP Integrity," (Reston, Virginia), pp. 720–729, Feb. 2019.
- [23] L.-T. Hsu, Y. Gu, and S. Kamijo, "NLOS Correction/Exclusion for GNSS Measurement Using RAIM and City Building Models," *Sensors*, vol. 15, pp. 17329–17349, July 2015.
- [24] S. Miura, S. Hisaka, and S. Kamijo, "GPS multipath detection and rectification using 3D maps," in *16th International IEEE Conference on Intelligent Transportation Systems (ITSC 2013)*, (The Hague, Netherlands), pp. 1528–1534, IEEE, Oct. 2013.
- [25] L.-T. Hsu, F. Chen, and S. Kamijo, "Evaluation of Multi-GNSSs and GPS with 3D Map Methods for Pedestrian Positioning in an Urban Canyon Environment," *IEICE Transactions on Fundamentals of Electronics, Communications and Computer Sciences*, vol. E98.A, no. 1, pp. 284–293, 2015.
- [26] H. Pesonen, "A Framework for Bayesian Receiver Autonomous Integrity Monitoring in Urban Navigation," *Navigation*, vol. 58, pp. 229–240, Sept. 2011.
- [27] S. Gupta and G. X. Gao, "Particle RAIM for Integrity Monitoring," (Miami, Florida), pp. 811–826, Oct. 2019.
- [28] D. N. Geary, G. J. McLachlan, and K. E. Basford, "Mixture Models: Inference and Applications to Clustering.," *Journal of the Royal Statistical Society. Series A (Statistics in Society)*, vol. 152, no. 1, p. 126, 1989.
- [29] A. P. Dempster, N. M. Laird, and D. B. Rubin, "Maximum Likelihood from Incomplete Data Via the EM Algorithm," *Journal of the Royal Statistical Society: Series B (Methodological)*, vol. 39, pp. 1–22, Sept. 1977.
- [30] P. A. M. Dirac, *The principles of quantum mechanics*. No. 27, Oxford university press, 1981.
- [31] Z. Chen and others, "Bayesian filtering: From Kalman filters to particle filters, and beyond," *Statistics*, vol. 182, no. 1, pp. 1–69, 2003.
- [32] M. Joerger and B. Pervan, "Kalman Filter Residual-Based Integrity Monitoring Against Measurement Faults," in *AIAA Guidance, Navigation, and Control Conference*, (Minneapolis, Minnesota), American Institute of Aeronautics and Astronautics, Aug. 2012.
- [33] L. Yu, "Research on GPS RAIM Algorithm Based on SIR Particle Filtering State Estimation and Smoothed Residual," *Appl. Mech. Mater.*, vol. 422, pp. 196–203, 2013.
- [34] X. Zhao, Y. Qian, M. Zhang, J. Niu, and Y. Kou, "An improved adaptive Kalman filtering algorithm for advanced robot navigation system based on GPS/INS," in *2011 IEEE International Conference on Mechatronics and Automation*, (Beijing, China), pp. 1039–1044, IEEE, Aug. 2011.
- [35] J. Vila and P. Schniter, "Expectation-maximization Gaussian-mixture approximate message passing," in *2012 46th Annual Conference on Information Sciences and Systems (CISS)*, (Princeton, NJ, USA), pp. 1–6, IEEE, Mar. 2012.
- [36] C. M. Bishop, *Pattern recognition and machine learning*. springer, 2006.
- [37] M. K. Simon, *Probability distributions involving Gaussian random variables: A handbook for engineers and scientists*. Springer Science & Business Media, 2007.
- [38] C. Gentner, S. Zhang, and T. Jost, "Corrigendum to "Log-PF: Particle Filtering in Logarithm Domain","" *Journal of Electrical and Computer Engineering*, vol. 2018, pp. 1–1, 2018.
- [39] F. Gustafsson, F. Gunnarsson, N. Bergman, U. Forssell, J. Jansson, R. Karlsson, and P.-J. Nordlund, "Particle filters for positioning, navigation, and tracking," *IEEE Transactions on Signal Processing*, vol. 50, pp. 425–437, Feb. 2002.
- [40] J. Cho, "On the enhanced detectability of GPS anomalous behavior with relative entropy," *Acta Astronautica*, vol. 127, pp. 526–532,

Oct. 2016.

- [41] M. Tossaint, J. Samson, F. Toran, J. Ventura-Traveset, M. Hernandez-Pajares, J. Juan, J. Sanz, and P. Ramos-Bosch, "The Stanford - ESA Integrity Diagram: A New Tool for The User Domain SBAS Integrity Assessment," *Navigation*, vol. 54, pp. 153–162, June 2007.
- [42] R. Van Der Merwe, A. Doucet, N. De Freitas, and E. A. Wan, "The unscented particle filter," in *Advances in neural information processing systems*, pp. 584–590, 2001.
- [43] F. G. Lether, "A Generalized Product Rule for the Circle," *SIAM Journal on Numerical Analysis*, vol. 8, pp. 249–253, June 1971.
- [44] A. Doucet, S. Godsill, and C. Andrieu, "On sequential Monte Carlo sampling methods for Bayesian filtering," *Statistics and Computing*, vol. 10, no. 3, pp. 197–208, 2000.
- [45] E. Wang, T. Pang, M. Cai, and Z. Zhang, "Fault Detection and Isolation for GPS RAIM Based on Genetic Resampling Particle Filter Approach," *TELKOMNIKA Indonesian Journal of Electrical Engineering*, vol. 12, pp. 3911–3919, May 2014.
- [46] K. Gunning, J. Blanch, T. Walter, L. de Groot, and L. Norman, "Integrity for Tightly Coupled PPP and IMU," (Miami, Florida), pp. 3066–3078, Oct. 2019.
- [47] P. Reisdorf, T. Pfeifer, J. Breßler, S. Bauer, P. Weissig, S. Lange, G. Wanielik, and P. Protzel, "The problem of comparable gnss results—an approach for a uniform dataset with low-cost and reference data," in *Proc. of Intl. Conf. on Advances in Vehicular Systems, Technologies and Applications (VEHICULAR)*, 2016.